EPJ manuscript No.
(will be inserted by the editor)

The low energy electronic band structure of bilayer graphene

E. McCann, D.S.L. Abergel, and Vladimir I. Fal'ko

Department of Physics, Lancaster University, Lancaster, LA1 4YB, UK

Abstract. We employ the tight binding model to describe the electronic band structure of bilayer graphene and we explain how the optical absorption coefficient of a bilayer is influenced by the presence and dispersion of the electronic bands, in contrast to the featureless absorption coefficient of monolayer graphene. We show that the effective low energy Hamiltonian is dominated by chiral quasiparticles with a parabolic dispersion and Berry phase 2π. Layer asymmetry produces a gap in the spectrum but, by comparing the charging energy with the single particle energy, we demonstrate that an undoped, gapless bilayer is stable with respect to the spontaneous opening of a gap. Then, we describe the control of a gap in the presence of an external gate voltage. Finally, we take into account the influence of trigonal warping which produces a Lifshitz transition at very low energy, breaking the isoenergetic line about each valley into four pockets.

1 Introduction

Following the fabrication of monolayer graphene [1], the observation of an unusual sequencing of quantum Hall effect plateaus [2] was explained in terms of Dirac-like chiral quasiparticles with Berry phase π [3–6]. Subsequently, bilayer graphene became the subject of intense interest in its own right. This followed the realisation that the low energy Hamiltonian of a bilayer describes chiral quasiparticles with a parabolic dispersion and Berry phase 2π [7] as confirmed by quantum Hall effect [8] and ARPES measurements [9].

The electronic band structure of bilayer graphene has been modelled using both density functional theory [10–12] and the tight binding model [13,7,14–17]. It has been predicted [7] that asymmetry between the on-site energies in the layers leads to a tunable gap between the conduction and valence bands. The dependence of the gap on external gate voltage has been modelled taking into account screening within the tight binding model [16,17,12] and such calculations appear to be in good agreement with ARPES measurements [9], observations of the quantum Hall effect [17], and density functional theory calculations [12].

In this paper, we describe the tight binding model of bilayer graphene and the corresponding low energy band structure in Section 2 . Section 3 explains how the optical absorption coefficient of bilayer graphene is influenced by the presence and dispersion of the electronic bands [18, 19], in contrast to the featureless absorption coefficient of monolayer graphene. We obtain the effective low energy Hamiltonian of bilayer graphene in Section 4 and we show that it is dominated by chiral quasiparticles with a parabolic dispersion and Berry phase 2π. Section 5 describes the opening of a gap in bilayer graphene due to layer asymmetry with a description of the band structure in Section 5.1, a demonstration that an undoped, gapless bilayer is stable with respect to the opening of a gap in Section 5.2, and a calculation using a self-consistent Hartree approximation to describe the control of the gap in the presence of external gates in Section 5.3. In Section 6 we take into account the effect of trigonal warping on the band structure and we present our conclusions in Section 7.

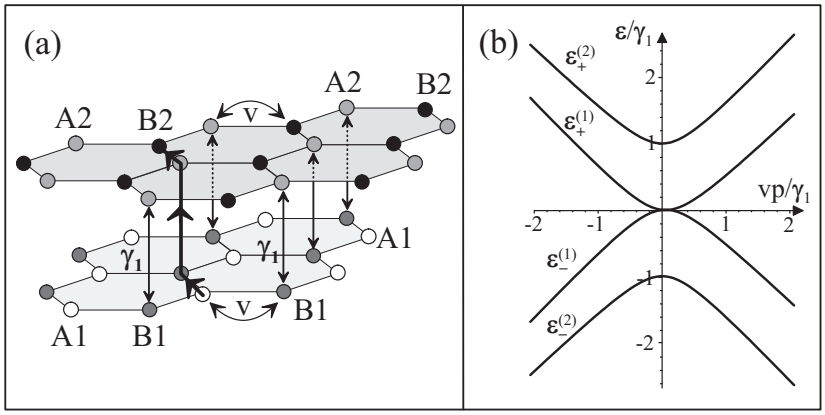

Fig. 1. (a) schematic of the bilayer lattice containing four sites in the unit cell: $A1$ (white circles) and $B1$ (grey) in the bottom layer, and $A2$ (grey) and $B2$ (black) in the top layer. (b) schematic of the low energy bands near the K point obtained by taking into account intralayer hopping with velocity v, $B1A2$ interlayer coupling γ_1, $A1B2$ interlayer coupling γ_3 [with $v_3/v = 0.1$] and zero layer asymmetry Δ.

2 The tight binding model of bilayer graphene

We consider bilayer graphene to consist of two coupled hexagonal lattices with inequivalent sites $A1, B1$ and $A2, B2$ on the bottom and top graphene sheets, respectively, arranged according to Bernal ($A2$-$B1$) stacking: as shown in Fig. 1(a), every $B1$ site in the bottom layer lies directly below an $A2$ site in the upper layer, but sites $A1$ and $B2$ do not lie directly below or above a site in the other layer. We employ the tight-binding model of graphite [20] by adapting the Slonczewski-Weiss-McClure parametrization [21,22] of relevant couplings in order to model bilayer graphene. In-plane hopping is parametrized by coupling $\gamma_{A1B1} = \gamma_{A2B2} \equiv \gamma_0$ and it leads to the in-plane velocity $v = (\sqrt{3}/2)a\gamma_0/\hbar$ where a is the lattice constant. In addition, we take into account the strongest inter-layer coupling, $\gamma_{A2B1} \equiv \gamma_1$, between pairs of $A2$-$B1$ orbitals that lie directly below and above each other. Such strong coupling produces dimers from these pairs of $A2$-$B1$ orbitals, leading to the formation of high energy bands. We also include weaker $A1$-$B2$ coupling $\gamma_{A1B2} \equiv \gamma_3$ that leads to an effective velocity $v_3 = (\sqrt{3}/2)a\gamma_3/\hbar$ where $v_3 \ll v$. Here, we write the Hamiltonian [7] near the centres of the valleys in a basis corresponding to wave functions $\Psi = (\psi_{A1}, \psi_{B2}, \psi_{A2}, \psi_{B1})$ in the valley K [23] and of $\Psi = (\psi_{B2}, \psi_{A1}, \psi_{B1}, \psi_{A2})$ in the valley $\tilde{K}$:

$$\mathcal{H} = \xi \begin{pmatrix} -\frac{1}{2}\Delta & v_3\pi & 0 & v\pi^\dagger \\ v_3\pi^\dagger & \frac{1}{2}\Delta & v\pi & 0 \\ 0 & v\pi^\dagger & \frac{1}{2}\Delta & \xi\gamma_1 \\ v\pi & 0 & \xi\gamma_1 & -\frac{1}{2}\Delta \end{pmatrix}, \tag{1}$$

where $\pi = p_x + ip_y$, $\pi^\dagger = p_x - ip_y$, $\mathbf{p} = (p_x, p_y)$ is the momentum measured with respect to the K point, $\xi = +1(-1)$ labels valley K ($\tilde{K}$). The Hamiltonian takes into account asymmetry $\Delta = \epsilon_2 - \epsilon_1$ between on-site energies in the two layers, $\epsilon_2 = \frac{1}{2}\Delta$, $\epsilon_1 = -\frac{1}{2}\Delta$.

At zero magnetic field, the Hamiltonian $\mathcal{H}$ has four valley-degenerate bands [7], $\epsilon_\pm^{(\alpha)}(\mathbf{p})$, $\alpha = 1, 2$, with

$$\epsilon^{(\alpha)2} = \frac{\gamma_1^2}{2} + \frac{\Delta^2}{4} + \left(v^2 + \frac{v_3^2}{2}\right)p^2 + (-1)^\alpha \left[\frac{\left(\gamma_1^2 - v_3^2p^2\right)^2}{4} + v^2p^2\left[\gamma_1^2 + \Delta^2 + v_3^2p^2\right] + 2\xi\gamma_1 v_3 v^2 p^3 \cos 3\phi\right]^{1/2}, \tag{2}$$

where $\mathbf{p} = p(\cos\phi, \sin\phi)$ is the momentum near the K point. They are plotted in Fig. 1(b) for $\Delta = 0$ and $v_3/v = 0.1$. The dispersion $\epsilon_\pm^{(2)}$ describes two bands with energies $\epsilon_+^{(2)} \geq \gamma_1$ and $\epsilon_-^{(2)} \leq \gamma_1$: they do not touch at the K point. These bands are the result of strong interlayer coupling $\gamma_{A2B1} \equiv \gamma_1$ which forms 'dimers' from pairs of $A2$-$B1$ orbitals that lie directly below and above each other [7].

The dispersion $\epsilon_1(p)$ describes low energy bands that touch at the K point in the absence of layer asymmetry $\Delta = 0$. In the intermediate energy range, $\frac{1}{4}\gamma_1(v_3/v)^2, |\Delta| < |\epsilon_1| < \gamma_1$, it can be approximated [7] with

$$\epsilon_\pm^{(1)} \approx \pm\tfrac{1}{2}\gamma_1 \left[\sqrt{1 + 4v^2p^2/\gamma_1^2} - 1\right]. \tag{3}$$

This corresponds to the effective mass for electrons near the Fermi energy in a 2D gas with density n,

$$m_c = p/(\partial\epsilon^{(1)}/\partial p) = \left(\gamma_1/2v^2\right)\sqrt{1 + 4\pi\hbar^2v^2n/\gamma_1^2}. \tag{4}$$

Eq. (3) interpolates between a linear spectrum $\epsilon^{(1)} \approx vp$ at high momenta and a quadratic spectrum $\epsilon^{(1)} \approx p^2/2m$, where $m = \gamma_1/2v^2$. Such a crossover happens at $p \approx \gamma_1/2v$, which corresponds to the carrier density $n^* \approx \gamma_1^2/(4\pi\hbar^2v^2)$. This is lower than the density at which the higher energy band $\epsilon^{(2)}$ becomes occupied $n^{(2)} \approx 2\gamma_1^2/(\pi\hbar^2v^2) \approx 8n^*$. Using experimental graphite values [22] gives $n^* \approx 4.36 \times 10^{12} cm^{-2}$ and $n^{(2)} \approx 3.49 \times 10^{13} cm^{-2}$. The estimated effective mass m is light: $m = \gamma_1/2v^2 \approx 0.054 m_e$.

3 Optical absorption of bilayer graphene

The electromagnetic (EM) field absorption in graphene at zero magnetic field has already been studied [24,18,25,26]. While the DC conductivity of monolayer graphene increases linearly with the carrier density [1,2,27], the real part of its high-frequency conductivity [24,25] is independent of the electron density in a wide spectral range above the threshold $\hbar\omega > 2|\epsilon_F|$, which determines a featureless absorption coefficient $g_1 = \pi e^2/\hbar c$. In contrast, we show that the bilayer absorption coefficient,

$$g_2 = (2\pi e^2/\hbar c)\, f_2(\omega), \tag{5}$$

reflects the presence and dispersion of two pairs of bands [18,19] as described in Section 2.

In a 2D electron gas with conductivity $\sigma(\omega) \ll c/2\pi$, absorption of an EM field $\mathbf{E}_\omega = \boldsymbol{\ell} E e^{-i\omega t}$ with polarisation $\boldsymbol{\ell}$ [$\boldsymbol{\ell}_\oplus = \sqrt{\frac{1}{2}}[\mathbf{l}_x - i\mathbf{l}_y]$ for right- and $\boldsymbol{\ell}_\ominus = \sqrt{\frac{1}{2}}[\mathbf{l}_x + i\mathbf{l}_y]$ for left-hand circularly polarised light arriving along the direction antiparallel to a magnetic field] can be characterised by the absorption coefficient $g \equiv E_i E_j^* \sigma_{ij}(\omega)/S$: the ratio between Joule heating and the energy flux $\mathbf{S} = c\mathbf{E} \times \mathbf{H}/4\pi = -S\mathbf{l}_z$ transported by the EM field. Using the Keldysh technique, we express

$$g = \frac{8e^2}{c\omega} \Re \int \frac{F d\epsilon}{N} \widehat{\mathrm{Tr}} \left\{ \hat{v}_i \ell_i \hat{G}^R(\epsilon) \hat{v}_j \ell_j^* \hat{G}^A(\epsilon + \omega) \right\},$$

where $\hat{\mathbf{v}} = \partial_{\mathbf{p}} \hat{H}$ is the velocity operator, $\widehat{\mathrm{Tr}}$ includes the summation both over the sublattice indices "tr" and over single-particle orbital states, N is the normalisation area of the sample and $F = n_F(\epsilon) - n_F(\epsilon + \omega)$ takes into account the occupancy of the initial and final states. Here we have included spin and valley degeneracy.

For a 2D gas in a zero magnetic field, the electron states are weakly scattered plane waves. Using the plane wave basis and the matrix form of the bilayer Hamiltonian $\mathcal{H}$ Eq. (1), we express the retarded/advanced Greens functions of electrons in the bilayer as $\hat{G}^{R/A}(\mathbf{p}, \epsilon) = \left[\epsilon \pm \frac{1}{2} i\hbar\tau^{-1} - \mathcal{H}(\mathbf{p})\right]^{-1}$ and $\widehat{\mathrm{Tr}} = \int d^2\mathbf{p} \frac{N}{(2\pi\hbar)^2} \mathrm{tr}$. After neglecting the renormalisation of the

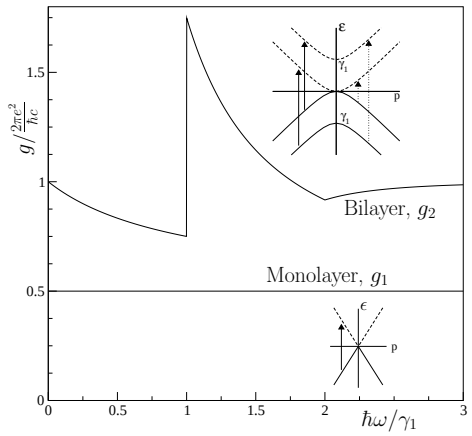

Fig. 2. Absorption coefficient of bilayer and monolayer graphene in the optical range of frequencies. The insets illustrate the quasiparticle dispersion branches in the vicinity of ϵ_F and possible optical transitions.

current operator by vertex corrections at $\omega\tau \gg 1$ and the momentum transfer from light (since $v/c \sim 3 \times 10^{-3}$), we reproduce [24,25] the constant absorption coefficient $g_1^{\parallel} = \pi e^2 \hbar c$ ($f_1 = \frac{1}{2}$) in monolayer graphene and arrive at the expression for the absorption coefficient of a bilayer for light polarised in the plane of the graphene sheet [28]:

$$g_2^{\parallel} = \frac{2\pi e^2}{\hbar c} f_2(\Omega), \qquad \Omega \equiv \frac{\hbar\omega}{\gamma_1} > \frac{2|\epsilon_{\rm F}|}{\gamma_1}, \tag{6}$$
$$f_2 = \frac{\Omega+2}{2(\Omega+1)} + \frac{\theta(\Omega-1)}{\Omega^2} + \frac{(\Omega-2)\theta(\Omega-2)}{2(\Omega-1)},$$

where $\theta(x<0)=0$ and $\theta(x>0)=1$. The above result agrees with the calculation by J. Nilsson *et al* [18] taken in the clean limit and T=0. The frequency dependence [29] of the bilayer optical absorption is illustrated in Fig.2, where an additional structure in the vicinity of $\hbar\omega = \gamma_1$ ($\gamma_1 \approx 0.4$eV [22]) is due to the electron-hole excitation between the low-energy band $\epsilon_{\pm}^{(1)}$ and the split band $\epsilon_{\pm}^{(2)}$. For the higher photon energies, $\hbar\omega \gtrsim 2\gamma_1$, the frequency dependence almost saturates at $f \approx 1$. Over the entire spectral interval shown in Fig.2, the absorption coefficient for the left- and right-handed light are the same, so that Eq. (6) is applicable [28] to light linearly polarised in the graphene plane.

We can also examine the reflection and transmission properties of graphene by including the imaginary part of the conductivity into our analysis. At zero temperature, the full conductivity is

$$\sigma(\omega) = \frac{4e^2}{\omega\hbar^2}\left[\mathcal{P}(\omega) - \mathcal{P}(0)\right], \tag{7}$$

where

$$\mathcal{P}(\omega) = \lim_{\delta\to 0} \iint \frac{d\epsilon\, d^2\mathbf{p}}{(2\pi)^3} \sum_{n,m} \frac{F_{nm}|v_{nm}|^2}{(\epsilon-\epsilon_m+i\delta)(\epsilon+\hbar\omega-\epsilon_n-i\delta)}.$$

Here m, n label initial and final states, respectively. Calculating these integrals gives the following explicit expressions for the conductivity:

$$\Re\sigma = \frac{e^2}{2\hbar} f_2(\Omega) \tag{8}$$

$$\Im\sigma = \frac{e^2}{2\pi\hbar}\left(\frac{\Omega\log\Omega}{1-\Omega^2} + \frac{2}{\Omega} - \frac{1}{\Omega^2}\log\left|\frac{1+\Omega}{1-\Omega}\right| \right. \\ \left. - \frac{1}{2}\frac{\Omega^2-2}{\Omega^2-1}\log\left|\frac{2+\Omega}{2-\Omega}\right| - \frac{1}{2}\frac{\Omega}{\Omega^2-1}\log|4-\Omega^2|\right) \quad (9)$$

The imaginary part has a divergence at $\Omega = 1$ and it is this (with the corresponding peak in the real part) which dominates the reflection properties. For comparison, the monolayer has $\Re\sigma = e^2/4\hbar$ and $\Im\sigma = 0$ at $T = 0$.

4 Effective low energy Hamiltonian

It is possible to obtain a low energy Hamiltonian that describes effective hopping between the non-dimer sites, $A1$-$B2$, *i.e.* those that do not lie directly below or above each other and are not strongly coupled by γ_1. This two component Hamiltonian was derived in [7] using Green's functions. Alternatively (and equivalently), one can view the eigenvalue equation of the four component Hamiltonian Eq. (1) as producing four simultaneous equations for components ψ_{A1}, ψ_{B2}, ψ_{A2}, ψ_{B1}. Eliminating the dimer state components ψ_{A2}, ψ_{B1} by substitution, and treating γ_1 as a large energy, gives the two component Hamiltonian [7] describing effective hopping between the $A1$-$B2$ sites:

$$\hat{H}_2 = -\frac{1}{2m}\begin{pmatrix} 0 & (\pi^\dagger)^2 \\ \pi^2 & 0 \end{pmatrix} + \hat{h}_w + \hat{h}_a; \quad (10)$$

$$\hat{h}_w = \xi v_3 \begin{pmatrix} 0 & \pi \\ \pi^\dagger & 0 \end{pmatrix}, \quad \text{where} \quad \pi = p_x + ip_y;$$

$$\hat{h}_a = -\xi\Delta\left[\tfrac{1}{2}\begin{pmatrix} 1 & 0 \\ 0 & -1 \end{pmatrix} - \frac{v^2}{\gamma_1^2}\begin{pmatrix} \pi^\dagger\pi & 0 \\ 0 & -\pi\pi^\dagger \end{pmatrix}\right].$$

The effective Hamiltonian $\hat{H}_2$ is applicable within the energy range $|\epsilon| < \frac{1}{4}\gamma_1$. In the valley K, $\xi = +1$, we determine $\Psi_{\xi=+1} = (\psi_{A1}, \psi_{B2})$, whereas in the valley $\tilde{K}$, $\xi = -1$, the order of components is reversed, $\Psi_{\xi=-1} = (\psi_{B2}, \psi_{A1})$. The Hamiltonian $\hat{H}_2$ describes two possible ways of $A1 \rightleftharpoons B2$ hopping. The first term takes into account $A1 \rightleftharpoons B2$ hopping via the $A2B1$ dimer state. Consider $A1$ to $B2$ hopping as illustrated with the thick solid line in Fig. 1(a). It includes three hops between sites: an intralayer hop from $A1$ to $B1$, followed by an interlayer transition via the dimer state $B1A2$, followed by an intralayer hop from $A2$ to $B2$. Since the two intralayer hops are both A to B, the first term in the Hamiltonian contains π^2 or $(\pi^\dagger)^2$ on the off-diagonal with the mass $m = \gamma_1/2v^2$ reflecting the energetic cost γ_1 of a transition via the dimer state. This term in the Hamiltonian yields a parabolic spectrum $\epsilon = \pm p^2/2m$ with $m = \gamma_1/2v^2$. It has been noticed [7] that quasiparticles described by it are chiral: their plane wave states are eigenstates of an operator $\sigma\mathbf{n}_2$ with $\sigma\mathbf{n}_2 = 1$ for electrons in the conduction band and $\sigma\mathbf{n}_2 = -1$ for the valence band, where $\mathbf{n}_2(\mathbf{p}) = (\cos(2\phi), \sin(2\phi))$ for $\mathbf{p} = (p\cos\phi, p\sin\phi)$. Quasiparticles described by the first term in $\hat{H}_2$ acquire a Berry phase 2π upon an adiabatic propagation along a closed orbit, thus charge carriers in a bilayer are Berry phase 2π quasiparticles, in contrast to Berry phase π particles in the monolayer of graphene [5].

The second term $\hat{h}_w$ in the Hamiltonian Eq. (10) describes weak direct $A1B2$ coupling, $\gamma_{A1B2} \equiv \gamma_3 \ll \gamma_1$, the effect of which will be discussed in Section 6. Other weaker tunneling processes [21] are neglected. The term $\hat{h}_a$ takes into account a possible asymmetry between the top and bottom layers (thus opening a gap $\sim \Delta$) that will be described in Section 5.

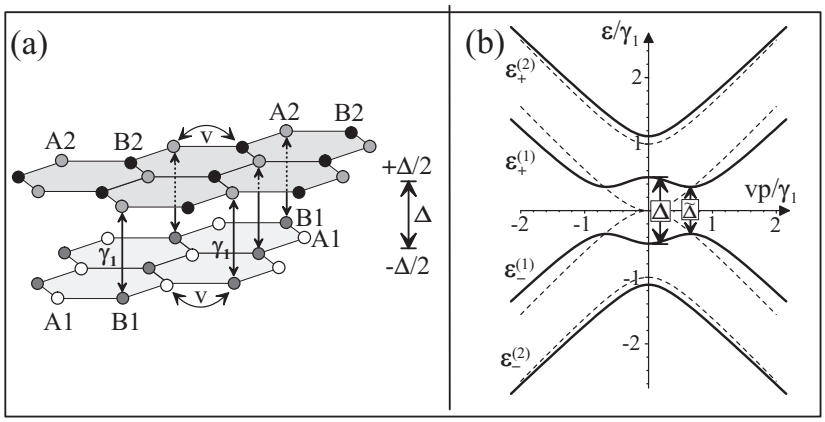

Fig. 3. (a) schematic of the bilayer lattice with different on-site energies in the two layers, $\epsilon_2 = \frac{1}{2}\Delta$, $\epsilon_1 = -\frac{1}{2}\Delta$. (b) schematic of the electronic bands near the K point in the presence of finite layer asymmetry Δ (for illustrative purposes a very large asymmetry $\Delta = \gamma_1$ is used) obtained by taking into account intralayer hopping with velocity v and $B1A2$ interlayer coupling γ_1, but neglecting $A1B2$ interlayer coupling γ_3. Dotted lines show the bands for zero asymmetry $\Delta = 0$.

5 Gap in the electronic band structure

5.1 Layer asymmetry and the gap in the electronic band structure

The parameter Δ in the Hamiltonian Eq. (1) takes into account asymmetry $\Delta = \epsilon_2 - \epsilon_1$ between on-site energies in the two layers, $\epsilon_2 = \frac{1}{2}\Delta$, $\epsilon_1 = -\frac{1}{2}\Delta$. The electronic bands near the K point, Eq. (2), are shown in Fig. 3(b) for a large value of the layer asymmetry Δ. For simplicity, we neglect $A1B2$ interlayer coupling γ_3:

$$\epsilon^{(\alpha)2} = \frac{\gamma_1^2}{2} + \frac{\Delta^2}{4} + v^2p^2 + (-1)^\alpha \sqrt{\frac{\gamma_1^4}{4} + v^2p^2\left(\gamma_1^2 + \Delta^2\right)}, \tag{11}$$

The energies of the bands exactly at the K point are $|\epsilon_\pm^{(2)}(p=0)| = \sqrt{\gamma_1^2 + \Delta^2/4}$ and $|\epsilon_\pm^{(1)}(p=0)| = |\Delta|/2$: the low energy bands, $\epsilon_\pm^{(1)}$, are split by the layer asymmetry Δ at the K point. Note that the "mexican hat" structure of the low energy bands means that the true value of the gap $\widetilde{\Delta}$ between the conduction and valence band occurs at finite momentum $p_g \neq 0$ away from the K point:

$$\widetilde{\Delta} = |\Delta| \frac{\gamma_1}{\sqrt{\gamma_1^2 + \Delta^2}}; \qquad p_g = \frac{|\Delta|}{2v}\sqrt{\frac{2\gamma_1^2 + \Delta^2}{\gamma_1^2 + \Delta^2}}. \tag{12}$$

For huge values of the asymmetry $|\Delta| \gg \gamma_1$, the gap saturates at $\widetilde{\Delta} \approx \gamma_1$ although for modest asymmetry values $|\Delta| \ll \gamma_1$, the relation is simply $\widetilde{\Delta} \approx |\Delta|$.

The electronic densities on the individual layers, n_1 and n_2, are given by an integral with respect to momentum $p = \hbar\,|\mathbf{k}|$ over the circularly symmetric Fermi surface, taking into account the relative weight of the wave functions:

$$n_{1(2)} = \frac{2}{\pi\hbar^2}\int p\,dp\left(\left|\psi_{A1(2)}(p)\right|^2 + \left|\psi_{B1(2)}(p)\right|^2\right), \tag{13}$$

where we have included a factor of four to take into account spin and valley degeneracy. By determining the wavefunction amplitudes on the four separate atomic sites we find

$$n_{1(2)} = \frac{1}{\pi\hbar^2}\int p\,dp\left[\frac{\epsilon \mp \Delta/2}{\epsilon}\frac{\left(\epsilon^2 - \Delta^2/4\right)^2 \mp 2v^2p^2\epsilon\Delta - v^4p^4}{\left(\epsilon^2 - \Delta^2/4\right)^2 + v^2p^2\Delta^2 - v^4p^4}\right], \tag{14}$$

where the minus (plus) sign is for the first (second) layer. The limits of integration are allowed values of momentum that, depending on the band in question and the value of the Fermi energy ϵ_F, are $p = 0$ or $p_\pm$ where

$$v^2 p_\pm^2 = \epsilon_F^2 + \frac{\Delta^2}{4} \pm \sqrt{\epsilon_F^2 \left(\gamma_1^2 + \Delta^2\right) - \frac{\gamma_1^2 \Delta^2}{4}}. \tag{15}$$

5.2 Stability of a gapless bilayer

We establish the stability of an undoped, gapless bilayer system with respect to the opening of a gap in the absence of external electric fields. This is done by estimating the energetic cost of opening a gap as determined by the charging energy E_c and comparing it with the energetic gain of opening a gap as given by the single particle energy E.

We estimate the charging energy by assuming that the excess electronic densities on the individual layers, n_1 and n_2, are uniformly distributed within infinitesimally thin 2d layers. Then, the charging energy is $E_c = Q^2/2C_b$ where $Q = en_1L^2 = -en_2L^2$ is the excess charge on one of the layers in the presence of finite asymmetry $\Delta = \epsilon_2 - \epsilon_1$, and $C_b = \varepsilon_r \varepsilon_0 L^2/c_0$ is the capacitance of a bilayer with interlayer separation c_0 and area L^2. For an undoped system, with Fermi energy $\epsilon_F = 0$ and zero excess total density $n_1 = -n_2$, we only need to consider the valence bands $\epsilon_-^{(1)}$ and $\epsilon_-^{(2)}$, Eq. (11). On integrating Eq. (14) from zero momentum to a large momentum p_∞, and using an expansion in Δ/γ_1, we find that the change in the density of the valence bands for finite Δ, as compared to $\Delta = 0$, is

$$n_{1(2)} \approx \pm \frac{\gamma_1 \Delta}{4\pi\hbar^2 v^2} \ln\left(\frac{4\gamma_1}{|\Delta|}\right). \tag{16}$$

Thus, on opening a gap in the spectrum, the charging energy may be estimated as

$$E_c \approx \frac{e^2}{32\pi^2 C_b} \left(\frac{L^2 \gamma_1 \Delta}{\hbar^2 v^2}\right)^2 \ln^2\left(\frac{4\gamma_1}{|\Delta|}\right). \tag{17}$$

The change in the single particle energy for finite Δ, as compared to $\Delta = 0$, may be estimated by integrating the valence bands energies $\epsilon_-^{(1)}$ and $\epsilon_-^{(2)}$, Eq. (11), with respect to momentum over the circularly symmetric Fermi surface:

$$E \approx \frac{2L^2}{\pi\hbar^2} \int p\, dp \left[\epsilon_-^{(1)}(\Delta) + \epsilon_-^{(2)}(\Delta) - \epsilon_-^{(1)}(0) - \epsilon_-^{(2)}(0)\right] \tag{18}$$

On integrating from zero momentum to a large momentum p_∞, and expanding in Δ/γ_1, the change in the single particle energy is

$$E \approx -\frac{\gamma_1}{8\pi} \left(\frac{L^2 \Delta^2}{\hbar^2 v^2}\right) \left[\frac{1}{2} + \ln\left(\frac{4\gamma_1}{|\Delta|}\right)\right]. \tag{19}$$

The logarithmic dependence of the density Eq. (16) appears as the square of the logarithm in the charging energy Eq. (17). Since the single particle energy Eq. (19) contains a single logarithm only, the large energetic cost of charging an undoped bilayer ensures stability with respect to the opening of a gap in the absence of an applied external electric field.

5.3 Controlling the gap using the electric field effect

The gap $\widetilde{\Delta}$ between the conduction and valence bands arises from layer asymmetry so that, in contrast to monolayer graphene, there is a possibility of tuning the magnitude of the gap using external gates. Indeed, a gate is routinely used in experiments to control the density of

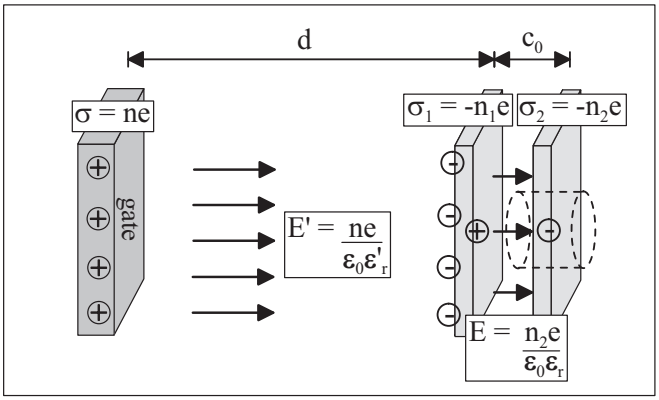

Fig. 4. Schematic of the graphene bilayer, with interlayer separation c_0, located a distance d from a parallel metallic gate. The gate voltage V_g induces a total excess electronic density $n = n_1 + n_2$ on the bilayer system where n_1 (n_2) is the excess density on the layer closest to (furthest from) the gate. The dashed line shows a Gaussian surface, from which it can be deduced that the magnitude of the electric field between the layers of the bilayer is $E = en_2/\varepsilon_r\varepsilon_0$.

electrons n on the bilayer system [1,2,8] and, in general, this will produce a simultaneous change in $\widetilde{\Delta}$. The dependence of $\widetilde{\Delta}$ on the density distribution of the bilayer arises from the Coulomb interaction between electrons, but the density distribution itself is dependent on the value of $\widetilde{\Delta}$ via the band structure. In the following we use a self-consistent Hartree approximation to determine the electronic distribution on the bilayer and the resulting band structure in the presence of an external gate.

As shown in Fig. 4, we consider the graphene bilayer, with interlayer separation c_0, to be located a distance d from a parallel metallic gate. The application of an external gate voltage $V_g = end/\varepsilon_r'\varepsilon_0$ induces a total excess electronic density $n = n_1 + n_2$ on the bilayer system where n_1 (n_2) is the excess density on the layer closest to (furthest from) the gate [we use the SI system of units]. Here ε_0 is the permittivity of free space, ε_r' is the dielectric constant of the material between the gate and the bilayer, and e is the electronic charge. We assume that the screening of the effective charge density $\rho_+ = en$ from the metallic gate is not perfect, leading to an excess electronic density n_2 on the layer furthest from the gate. We also assume that the excess densities n_1 and n_2 are uniformly distributed within infinitesimally thin 2d layers. Considering a Gaussian surface, such as that shown with the dashed lines in Fig. 4, shows that the excess density n_2 gives rise to an electric field with magnitude $E = en_2/\varepsilon_r\varepsilon_0$ between the layers where ε_r is the nominal dielectric constant of the bilayer. There is a corresponding change in potential energy $\Delta U = e^2 n_2 c_0/\varepsilon_r\varepsilon_0$ that determines the layer asymmetry [16]:

$$\Delta(n) = \epsilon_2 - \epsilon_1 \equiv \Delta_0 + \frac{e^2 n_2 c_0}{\varepsilon_r \varepsilon_0}. \tag{20}$$

In terms of the capacitance of a bilayer of area L^2, $C_b = \varepsilon_r\varepsilon_0 L^2/c_0$, this may be written $\Delta(n) = \Delta_0 + e^2 n_2 L^2/C_b$. In order to generalise the description, we include a bare asymmetry parameter Δ_0 to take into account the possibility of finite bilayer asymmetry at zero excess density that may arise in the presence of a substrate or an additional transverse electric field, created, for example, by employing multiple gates.

The aim of the calculation is to self consistently calculate the excess densities n_1, n_2, $n = n_1 + n_2$, Eq. (14), and the gap Δ, Eq. (20). This is done numerically and analytically (the latter within certain regimes as explained below). The calculation proceeds by first determining the initial density on each layer, $n_1^{(0)}$ and $n_2^{(0)}$, in the absence of an external gate voltage, assuming the Fermi energy to be located at $\epsilon = 0$. This is done self-consistently by performing the integral Eq. (14) over the two valence bands with the relation $\Delta(0) = \Delta_0 + e^2 n_2^{(0)} c_0/\varepsilon_r\varepsilon_0$ to

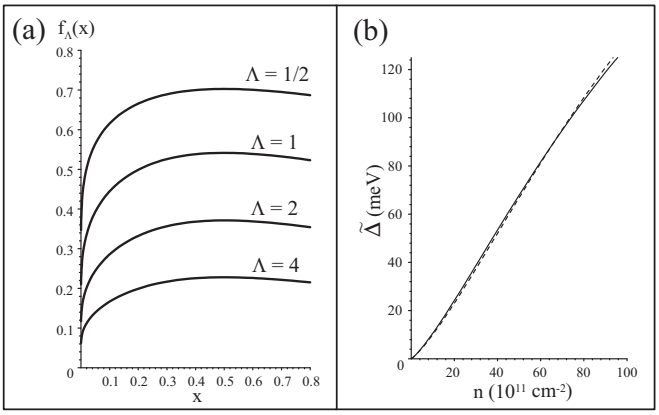

Fig. 5. (a) dependence of the function $f_\Lambda(x)$, Eq. (22), on the argument x for different values of the screening parameter Λ, (b) numerically calculated dependence $\tilde{\Delta}(n)$ (solid line) compared with analytic expression (dashed line) using Eqs. (12,22) and typical parameters [22]. For these values of density $\tilde{\Delta} \approx \Delta$.

determine the gap at zero voltage $\Delta(0)$. Then, we proceed to the case where an external gate voltage produces excess total density on the bilayer system. It is convenient to define a Fermi energy ϵ_F and self-consistently determine the density corresponding to it because the value of ϵ_F dictates which bands are fully or partially occupied. Note that, when performing the momentum integral Eq. (14) over partially occupied bands, the lower limit is 0 or p_- and the upper is p_- or p_+, depending on the band in question. This allows a self-consistent calculation of the excess densities n_1, n_2, $n = n_1 + n_2$, and of the gap Eq. (20).

It is possible to obtain an analytic expression for the asymmetry gap Δ in the limit $\gamma_1, \epsilon_F \gg |\Delta|$ by evaluating the density on each layer Eq. (14) using an expansion in Δ/γ_1. For simplicity, we consider the Fermi energy to lie in the interval $|\Delta|/2 < |\epsilon_F| < \gamma_1$ so that either the band just above or just below zero energy is partially occupied. On integrating Eq. (14) from zero momentum to $p_F = p_+$, we find the densities in the partially occupied bands to be

$$n_{1(2)} \approx \frac{\mathrm{sgn}\,(\epsilon_F)\, p_F^2}{2\pi\hbar^2} \pm \frac{\gamma_1 \Delta}{2\pi\hbar^2 v^2}\left[\frac{\epsilon_0}{\gamma_1} + \frac{\epsilon_0^2}{\gamma_1^2} - \frac{1}{2}\ln\left(\frac{4\epsilon_0}{|\Delta|}\right)\right],$$

where $\epsilon_0 = (\gamma_1/2)[\sqrt{1 + 4v^2 p_F^2/\gamma_1^2} - 1]$. In order to determine the total densities on the layers, we must take into account the redistribution of density within the valence bands for $\Delta \neq 0$ as compared to the $\Delta = 0$ case, as given by $\pm\gamma_1\Delta/\left(4\pi\hbar^2 v^2\right)\ln\left(4\gamma_1/|\Delta|\right)$ [Eq. (16)], leading to

$$n_{1(2)} \approx \frac{\mathrm{sgn}\,(\epsilon_F)\, p_F^2}{2\pi\hbar^2} \pm \frac{\gamma_1 \Delta}{2\pi\hbar^2 v^2}\left[\frac{\epsilon_0}{\gamma_1} + \frac{\epsilon_0^2}{\gamma_1^2} - \frac{1}{2}\ln\left(\frac{\epsilon_0}{\gamma_1}\right)\right],$$

so that $n = n_1 + n_2 \approx \mathrm{sgn}\,(\epsilon_F)\, p_F^2/\left(\pi\hbar^2\right)$. If we assume that $|\Delta| \ll \{|\epsilon_F|, \gamma_1\}$ so that $v^2 p_F^2 \approx \epsilon_F^2 + \gamma_1|\epsilon_F|$ [for $p_F = p_+$ Eq. (15)], then ϵ_0 is approximately independent of Δ, and we may use the expression $\Delta(n) = \Delta_0 + e^2 n_2 L^2/C_b$ to find an approximation for the gap in terms of the total density and parameter values [16]:

$$\Delta \approx \frac{\Delta_0 + e^2 L^2 n/(2C_b)}{1 + \Lambda\left[(\epsilon_0/\gamma_1) + (\epsilon_0^2/\gamma_1^2) - \frac{1}{2}\ln\left(\epsilon_0/\gamma_1\right)\right]}, \tag{21}$$

where the dimensionless parameter $\Lambda = e^2 L^2 \gamma_1/(2\pi\hbar^2 v^2 C_b)$. The expression Eq. (21) is valid for intermediate densities $|\Delta|, |\Delta_0| \ll \epsilon_F < \gamma_1$ where $\epsilon_F \approx \pm\epsilon_0$ [at very low density it incorrectly predicts $\Delta(0) = 0$ for $\Delta_0 \neq 0$].

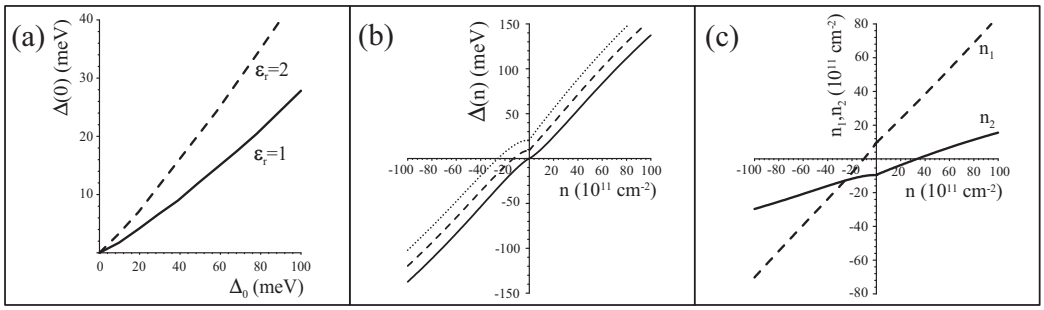

Fig. 6. Numerical evaluation of (a) $\Delta(0)$ as a function of Δ_0 for $\varepsilon_r = 1$ (solid line) and $\varepsilon_r = 2$ (dashed), (b) the bilayer asymmetry $\Delta(n)$ for different values of the bare asymmetry $\Delta_0 = 0$ (solid line), $\Delta_0 = 0.1\gamma_1 = 39$meV (dashed line) and $\Delta_0 = 0.2\gamma_1 = 78$meV (dotted line), using typical parameter values [22], (c) layer densities n_2 (solid) and n_1 (dashed) as a function of n for $\Delta_0 = 0.2\gamma_1 = 78$meV.

For zero bare asymmetry parameter $\Delta_0 = 0$, and for moderately low density, $4\pi\hbar^2 v^2|n| \ll \gamma_1^2$, the expression Eq. (21) reduces to

$$\Delta = \frac{e^2 L^2 n}{2C_b} f_\Lambda\left(\frac{\hbar^2 v^2 \pi |n|}{\gamma_1^2}\right); \qquad f_\Lambda(x) \approx \frac{1}{1+\Lambda\left(x - \frac{1}{2}\ln x\right)}. \tag{22}$$

The function $f_\Lambda(x)$ is plotted in Fig. 5(a) for different values of the dimensionless parameter Λ. The parameter Λ describes the effectiveness of the screening of the bilayer. The limit $\Lambda \to 0$ describes poor screening when the density on each layer is equal to $n/2$ whereas for $\Lambda \to \infty$ there is excellent screening, the density lies solely on the layer closest to the external gate and $\Delta = 0$. Note that $f_\Lambda(x) \to 0$ as $x \to 0$ because of the logarithm, meaning that the effectiveness of screening increases dramatically at very low density. Note also that, in this calculation, we neglected the role of additional weak couplings, such as $A1$-$B2$ coupling γ_3 that results in trigonal warping, Section 6, and is relevant at low density $n \sim 1 \times 10^{11}\text{cm}^{-2}$. Indeed, trigonal warping should result in a small overlap between the conduction and valence band of ≈ 2meV.

Unless explicitly stated otherwise, we use $c_0 = 3.35$Å for the interlayer separation and $\varepsilon_r = 1$ for the dielectric constant of the bilayer [22]. The latter agrees with the prediction for other low dimensional structures [30], but is smaller than the value for bulk graphite $\varepsilon_r \approx 2.4$ [31]. Using typical experimental parameters [22] we find $\Lambda \approx 1.3$. The numerically calculated dependence $\Delta(n)$ is shown in Fig. 5(b) (solid line) for typical experimental parameters in the case that the asymmetry gap $\Delta = 0$ at zero excess density and it is compared with the analytic expression (dashed line) Eq. (22). It shows that the addition of density $n \sim 10^{12}\text{cm}^{-2}$ yields a gap $\Delta \sim 10$meV.

The influence of finite bare asymmetry Δ_0 is illustrated in Fig. 6. Naturally, it results in a finite asymmetry $\Delta(0)$ at zero density but, as a result of screening, the asymmetry at zero density $\Delta(0)$ is smaller than the bare asymmetry Δ_0. Fig. 6(a) shows $\Delta(0)$ as a function of Δ_0 for two values of the dielectric constant of the bilayer: $\varepsilon_r = 1$ (solid line) and $\varepsilon_r = 2$ (dashed). This demonstrates that the gap $\Delta(0)$ increases with the dielectric constant, as expected from the screening parameter $\Lambda = e^2 L^2 \gamma_1/(2\pi\hbar^2 v^2 C_b)$. Figure 6(b) shows a calculation of $\Delta(n)$ using typical experimental parameters [22] for different values of the bare asymmetry Δ_0. The main effect of finite Δ_0 (dashed and dotted lines) is to shift the plot $\Delta(n)$ with respect to the $\Delta_0 = 0$ case (solid line). Fig. 6(c) shows the variation of the individual layer densities n_1 and n_2 for finite Δ_0.

Recently, gaps up to 200meV have been achieved by electronic doping [9]. Alternatively, it would be possible to independently control the density and the gap by employing both a top and a bottom gate. For example, potential $+V_g$ applied to a bottom gate at a distance d from the bilayer combined with potential $-V_g$ applied to a top gate at a distance d (for simplicity, we consider the symmetric case) would lead to no net density on the bilayer, $n_2 = -n_1$, but a screening of the external gate voltage as in Fig. 6(a) according to Eq. (20), $\Delta(0) = \Delta_0 +$

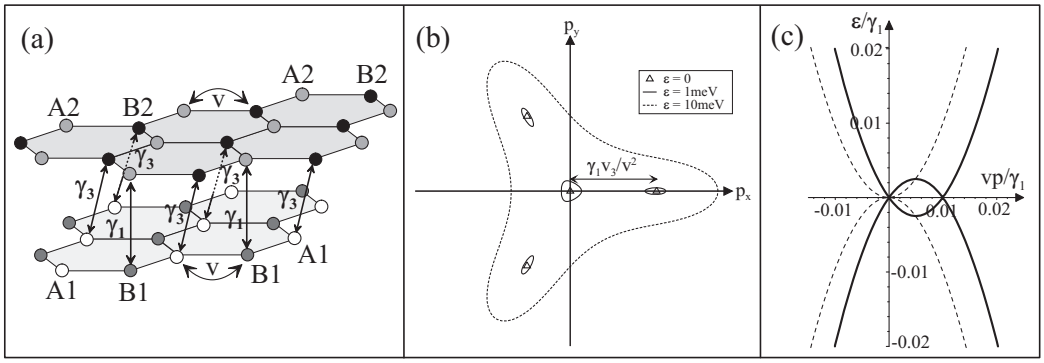

Fig. 7. (a) schematic of the bilayer lattice showing the additional interlayer coupling $A1B2$ parameterised by γ_3, (b) schematic of the Fermi line in the valley K, $\xi = 1$, for different values of the Fermi energy. Note that the asymmetry of the Fermi line at the other valley, $\xi = -1$, is inverted, (c) the low energy bands plotted along the line $p_y = 0$. They are obtained by taking into account intralayer hopping with velocity v, $B1A2$ interlayer coupling γ_1, $A1B2$ interlayer coupling γ_3 [with $v_3/v = 0.1$] and zero layer asymmetry Δ. Dashed lines show the bands obtained by neglecting γ_3 [*i.e.* with $v_3/v = 0$].

$e^2 n_2 L^2/C_b$, where the bare asymmetry parameter is $\Delta_0 = eV_g(c_0/d)(\varepsilon_r'/\varepsilon_r)$. Taking $d = 300$nm and $\varepsilon_r' = 3.9$ for SiO_2, $c_0 = 3.35$Å and $V_g = 20$V yields $\Delta_0 \approx 87$meV for $\varepsilon_r = 1$ corresponding to $\Delta(0) \sim 25$meV [using Fig. 6(a)] or it gives $\Delta_0 \approx 44$meV for $\varepsilon_r = 2$ corresponding to $\Delta(0) \sim 18$meV.

6 Trigonal warping

The $A1$-$B2$ coupling $\gamma_{A1B2} \equiv \gamma_3$ is shown in Fig. 7(a). It leads to the effective velocity $v_3 = (\sqrt{3}/2)a\gamma_3/\hbar$ where $v_3 \ll v$ that appears in the expression for the energies Eq. (2). In a similar way to bulk graphite [21,32], the effect of coupling γ_3 is to produce trigonal warping, which deforms the isoenergetic lines along the directions $\varphi = \varphi_0$, as shown in Fig. 7(b). For the valley K, $\varphi_0 = 0$, $\frac{2}{3}\pi$ and $\frac{4}{3}\pi$, whereas for $\tilde{K}$, $\varphi_0 = \pi$, $\frac{1}{3}\pi$ and $\frac{5}{3}\pi$. The effective low energy Hamiltonian Eq. (10) yields the following energy for $\Delta = 0$,

$$\epsilon^{(1)2} \approx (v_3 p)^2 - \frac{\xi v_3 p^3}{m}\cos(3\phi) + \left(\frac{p^2}{2m}\right)^2, \tag{23}$$

which agrees with Eq. (2) in the low energy limit $|\epsilon| \ll \gamma_1$. At very low energies $|\epsilon| < \epsilon_L = \frac{1}{4}\gamma_1(v_3/v)^2 \approx 1$meV, the effect of trigonal warping is dramatic. It leads to a Lifshitz transition: the isoenergetic line is broken into four pockets, which can be referred to as one "central" and three "leg" parts [32,7]. The central part and leg parts have minimum $|\epsilon| = \frac{1}{2}|\Delta|$ at $p = 0$ and at $|p| = \gamma_1 v_3/v^2$, angle φ_0, respectively. For $v_3 \ll v$, we find [7,22] that the separation of the 2D Fermi line into four pockets would take place for very small carrier densities $n < n_L \sim (v_3/v)^2 n^* \sim 1 \times 10^{11} cm^{-2}$. In this estimation of n_L, the constant of proportionality is of order 1 as determined by the strongly warped shape of the Fermi line at the Lifshitz transition. For $n < n_L$, the central part of the Fermi surface is approximately circular with area $\mathcal{A}_c \approx \pi\epsilon^2/(\hbar v_3)^2$, and each leg part is elliptical with area $\mathcal{A}_\ell \approx \frac{1}{3}\mathcal{A}_c$. The low energy part of the band structure is plotted in Fig. 7(c) along the line $p_y = 0$. Taking the line $p_y = 0$, Figs. 7(b),(c), $\phi = 0$, at the first valley $\xi = 1$ gives $\epsilon_\pm^{(1)} = \pm|v_3 p - p^2/(2m)|$. It shows that, at zero energy, the leg pocket of the Fermi surface develops at $p = 2mv_3 = \gamma_1 v_3/v^2$, Fig. 7(b), and that the overlap between the conduction and valence bands, Fig. 7(c), is given by $2\epsilon_L \approx (\gamma_1/2)(v_3/v)^2 \approx 2$meV [15] using $\gamma_1 \approx 0.4$eV and $v_3/v \approx 0.1$.

7 Conclusions

We described the tight binding model of bilayer graphene and the resulting low energy electronic band structure. The optical absorption coefficient of a bilayer displays features related to the band structure on the energy scale of the order of the interlayer coupling $\gamma_1 \approx 0.4$eV [18, 19], in contrast to the featureless absorption coefficient of monolayer graphene. At much lower energies, $\epsilon_L \sim 1$meV, trigonal warping of the band structure has a dramatic effect, producing a Lifshitz transition in which the isoenergetic line about each valley is broken into four pockets.

Layer asymmetry creates a gap between the conduction and valence bands: bilayer graphene is a semiconductor with a tuneable gap of up to about 0.4eV. However, by comparing the charging energy with the single particle energy, it is possible to show that an undoped, gapless bilayer is stable with respect to the spontaneous opening of a gap. A simple self consistent Hartree approximation was used to take into account screening an external gate, employed primarily to control the density n of electrons on the bilayer, resulting in a density dependent gap $\Delta(n)$. For the typical experimental range of densities shown in Fig. 5(b) the dependence of the asymmetry gap $\Delta(n)$ is roughly linear with n with the addition of density $n \sim 10^{12}\text{cm}^{-2}$ yielding a gap $\Delta \sim 10$meV. Control of the gap has been modelled using the tight binding model [16,17,12] and such calculations appear to be in good agreement with ARPES measurements [9], observations of the quantum Hall effect [17], and density functional theory calculations [12]. The use of a single gate modulates the density and the gap simultaneously, but it should be possible to independently control the density and the gap by employing both a top and a bottom gate. This suggests a route to new nanoelectronic devices defined within a single sheet of gated bilayer graphene.

The authors thank I. Aleiner, A. K. Geim, K. Kechedzhi, P. Kim, K. Novoselov, and L. M. K. Vandersypen for useful discussions and EPSRC for financial support.

References

1. K.S. Novoselov, A.K. Geim, S.V. Morozov, D. Jiang, Y. Zhang, S.V. Dubonos, I.V. Grigorieva, and A.A. Firsov, Science **306**, (2004) 666.
2. K.S. Novoselov, A.K. Geim, S.V. Morozov, D. Jiang, M.I. Katsnelson, I.V. Grigorieva, S.V. Dubonos, and A.A. Firsov, Nature **4**38, (2005) 197; Y.B. Zhang, Y.W. Tan, H.L. Stormer, and P. Kim, Nature **4**38, (2005) 201.
3. D. DiVincenzo and E. Mele, Phys. Rev. B **29**, (1984) 1685.
4. G.W. Semenoff, Phys. Rev. Lett. **53**, (1984) 2449.
5. F.D.M. Haldane, Phys. Rev. Lett. **61**, (1988) 2015; Y. Zheng and T. Ando, Phys. Rev. B **65**, (2002) 245420; V. P. Gusynin and S. G. Sharapov, Phys. Rev. Lett. **95**, (2005) 146801; N.M.R. Peres, F. Guinea, and A.H. Castro Neto, Physical Review B 73, (2006) 125411; A.H. Castro Neto, F. Guinea, and N.M.R. Peres, Phys. Rev. B **73**, (2006) 205408.
6. T. Ando, T. Nakanishi, R. Saito, J. Phys. Soc. Japan **67**, (1998) 2857.
7. E. McCann and V. I. Fal'ko, Phys. Rev. Lett. **96**, (2006) 086805.
8. K. S. Novoselov, E. McCann, S.V. Morozov, V.I. Fal'ko, M.I. Katsnelson, U. Zeitler, D. Jiang, F. Schedin, and A.K. Geim, Nature Physics **2**, (2006) 177.
9. T. Ohta, A. Bostwick, T. Seyller, K. Horn, and E. Rotenberg, Science **313**, 951 (2006).
10. S.B. Trickey, G.H.F. Diercksen, and F. Müller-Plathe, Astrophys. J. **336**, (1989) L37; S.B. Trickey, F. Müller-Plathe, G.H.F. Diercksen, and J.C. Boettger, Phys. Rev. B **45**, (1992) 4460.
11. S. Latil and L. Henrard, Phys. Rev. Lett. **97**, 036803 (2006).
12. H. Min, B.R. Sahu, S.K. Banerjee, and A.H. MacDonald, cond-mat/0612236.
13. K. Yoshizawa, T. Kato, and T. Yamabe, J. Chem. Phys. **105**, (1996) 2099; T. Yumura and K. Yoshizawa, Chem. Phys. **279**, (2002) 111.
14. C.L. Lu, C.P. Chang, Y.C. Huang, R.B. Chen, and M.L. Lin, Phys. Rev. B **73**, (2006) 144427; J. Nilsson, A. H. Castro Neto, N. M. R. Peres, and F. Guinea, Phys. Rev. B **73**, (2006) 214418; M. Koshino and T. Ando, Phys. Rev. B **73**, 245403 (2006); F. Guinea, A. H. Castro Neto, and N. M. R. Peres, Phys. Rev. B **73**, (2006) 245426; M. I. Katsnelson, Eur. Phys. J. B **51**, (2006) 157; **52**, (2006) 151;
15. B. Partoens and F. M. Peeters, Phys. Rev. B **74**, (2006) 075404.

16. E. McCann, Phys. Rev. B **74**, (2006) 161403.
17. E.V. Castro, K.S. Novoselov, S.V. Morozov, N.M.R. Peres, J.M.B. Lopes dos Santos, J. Nilsson, F. Guinea, A.K. Geim, and A.H. Castro Neto, cond-mat/0611342.
18. J. Nilsson, A.H. Castro Neto, F. Guinea and N.M.R. Peres, Phys. Rev. Lett. **97**, (2006) 266801.
19. D.S.L. Abergel and V.I. Fal'ko, cond-mat/0610673.
20. P.R. Wallace, Phys. Rev. **71**, (1947) 622; J.C. Slonczewski and P.R. Weiss, Phys. Rev. **109** (1958) 272.
21. M.S. Dresselhaus and G. Dresselhaus, Adv. Phys. **51**, (2002) 1; R.C. Tatar and S. Rabii, Phys. Rev. B **25**, (1982) 4126; J.-C. Charlier, X. Gonze, and J.-P. Michenaud, Phys. Rev. B **43**, (1991) 4579.
22. We use $\gamma_1 = 0.39eV$ [21,9], $v_3/v = 0.1$, $v = 8.0 \times 10^5 m/s$ [2], $c_0 = 3.35$Å, and $\varepsilon_r = 1$.
23. Corners of the hexagonal Brilloin zone are $\mathbf{K}_\xi = \xi(\frac{4}{3}\pi a^{-1}, 0)$, where $\xi = \pm 1$ and a is the lattice constant.
24. V. Gusynin, S. Sharapov, J. Carbotte, Phys. Rev. Lett. **96**, (2006) 256802; V. Gusynin and S. Sharapov, Phys. Rev. B **73**, (2006) 245411.
25. L. Falkovsky and A. Varlamov, cond-mat/0606800.
26. J. Cserti, Phys. Rev. B **75**, (2007) 033405.
27. K. Nomura and A.H. MacDonald, Phys. Rev. Lett. **96**, (2006) 256602; T. Ando, J. Phys. Soc. Jpn. **75**, (2006) 074716; V. Cheianov and V.I. Fal'ko, Phys. Rev. Lett. **97**, (2006) 226801.
28. In contrast to monolayer graphene, a weak absorption of light polarised perpendicular to the bilayer is possible. A pertubation $\sigma_z e E_z d/2$ distinguishes between the on-site energies in the top and bottom layers separated by spacing d, which leads to weak absorption $g_2^z = (2\pi e^2/\hbar c) f_2^z$,

$$f_2^z = a_z^2 \Omega \ \tfrac{1}{\Omega+1} + \tfrac{\theta(\Omega-2)}{\Omega-1} \ , \quad \Omega \equiv \hbar\omega/\gamma_1;$$

$$f_2^z(B,\omega) = \frac{a_z^2}{\pi} \sum_{n\geq 2} \frac{\tau\omega}{\tau^2\omega_c^2(\frac{\omega}{\omega_c} - 2\sqrt{n^2-n})^2 + 1}$$

where the constant $a_z = \gamma_1 d/2\hbar v \sim 10^{-1}$, and the magneto-absorption spectrum at $\hbar\omega < \frac{1}{4}\gamma_1$ involves $\varepsilon_{n-} \to \varepsilon_{n+}$ inter-LL transitions.
29. For $\hbar\omega \ll \frac{1}{4}\gamma_1$ this result transforms into $f_2 = 1$ suggested by J.Cserti [26] for the microwave absorption in bilayer graphene. However one should be aware that Eq. (6) and conclusions of Ref. [26] cannot be applied to $\hbar\omega \lesssim \epsilon_{\rm L} = \frac{1}{4}\gamma_1(v_3/v)^2 \sim 1$meV. At $\epsilon_{\rm F} \approx \epsilon_{\rm L}$, trigonal warping term causes a Lifshitz transition in the topology of the Fermi line in each valley as explained in Section 6.
30. F. Léonard and J. Tersoff, Appl. Phys. Lett. **81**, (2002) 4835.
31. K. W.-K. Shung, Phys. Rev. B **34**, (1986) 979; E. A. Taft and H. R. Philipp, Phys. Rev. **138**, (1965) A197.
32. G. Dresselhaus, Phys. Rev. B **10**, (1974) 3602; K. Nakao, J. Phys. Soc. Japan, **40**, (1976) 761; M. Inoue, J. Phys. Soc. Japan, **17**, (1962) 808; O.P. Gupta and P.R. Wallace, Phys. Stat. Sol. B **54**, (1972) 53.